Dynamics in vibrofluidized beds: A diffusing wave spectroscopy study

Marlo Kunzner,[1] Christopher Mayo,[1] Matthias Sperl,[1,2,*] and Jan Philipp Gabriel[1,†]
[1]*Institut für Materialphysik im Weltraum, Deutsches Zentrum für Luftund Raumfahrt (DLR), 51170 Cologne, Germany*
[2]*Department for Theoretical Physics, University of Cologne, Zülpicher Strasse 77, 50937 Cologne, Germany*

(Received 1 March 2025; accepted 3 July 2025; published 4 August 2025)

We demonstrate the densification of a granular model system of 130 μm polystyrene spheres over time by shaking with varying excitation amplitudes or effective temperatures. This densification is quantified by the mean-square displacement (MSD), which is measured by diffuse wave spectroscopy (DWS) of a sinusoidally excited vibrating fluidized granular bed. The DWS method also extracts the inherent heterogeneous dynamics of the system in the bulk and at the wall. Through an empirical model-based extraction, we obtain the ballistic and diffusive time constants, as well as caging sizes, which were found to depend on temperature and density. The results obtained from this study reveal a subdiffusive power-law behavior in the MSD, indicating an arrest of motion and potentially a glassy system, especially in cases where the excitation is low to moderate compared to gravity. The extracted MSD caging sizes are two orders smaller than the Lindeman length found in colloidal systems.

DOI: 10.1103/f3m6-b42t

I. INTRODUCTION

In everyday life, it is common to observe granular matter in motion. The movement of wind, for example, can be seen in the drifting of sand dunes or the occurrence of sandstorms. Within industrial contexts, another example of granular matter in motion is the passage of wheat grains through a silo. The perspective of material science addresses the diverse forms of motion within granular systems, which bear resemblance to the solid, liquid, and gas phases characterized in thermodynamics [1–4]. A primary area of interest is the transition from liquid-like states to solid-like states, which can be described as a glass transition [5,6]. This transition, as well as the dynamics of granular media in general, is in some respects more complicated than in atomic matter, due to the many interactions such as electrostatics, friction, dissipation, and gravity [2–4,7,8]. Many macroscopic descriptions of the behavior of powders exist, but looking at interparticle dynamics is often complicated, as powders are dense and opaque [2,4,9,10]. Here we consider a granular model system of polystyrene spheres driven by sinusoidal oscillating agitation. To provide a good statistical description of the system and take advantage of the opaqueness, we use diffusive wave spectroscopy (DWS) as a method to measure intensity correlation functions and then subsequently calculate the mean-square displacements (MSDs) of our particles under certain assumptions [11,12]. DWS has previously been used to study dry gas fluidized beds and granular flows [13–15] and vibrated suspensions [16,17]. Some studies have investigated, similarly to ours, a dry vibro-fluidized bed of grains with DWS [18–21]. However, we focus on exploring the influence of vibro-fluidized beds on the dynamics of granular media in the full available spectral DWS range by modeling the agitation. DWS can fully utilize its key features: the ability to measure high spatial and temporal resolution with regard to a large number of particle movements in this system. This in turn enables a comparison of this system to funnel and gas-fluidized beds. The findings from this study will serve as a solid foundation for future research, including experiments conducted under microgravity conditions on the International Space Station [22], as well as extending the investigation to different agitation methods, particle sizes, and frictional properties.

II. METHODS

In this section we will first introduce details about the experiment and the sample and, second, explain the DWS method and the adaptations for agitated dry grains.

A. Experimental details

The setup comprises a $15 \times 15 \times 5\,\mathrm{mm}^3$ sample cell containing 0.602 g of 130 μm polystyrene particles (Dynoseeds 140, mean size 130 μm, the distribution of particle sizes is in [23]) mounted on a voice coil (VC) Visaton EX 80 S and a laser wavelength of $\lambda = 532$ nm (Coherent Verdi G5 SLM), as is shown in Fig. 1. The container is shaken via an oscillation from the voice coil. This supplies the system with energy, thereby agitating the system. The laboratory is not humidity controlled, but the sample cell is sealed airtight [24]. The green laser light is scattered multiple times and detected via single-mode fibers and polarizers connected to avalanche photodiodes (APDs) in backscattered and transmission

*Contact author: Matthias.Sperl@dlr.de
†Contact author: Jan.Gabriel@dlr.de

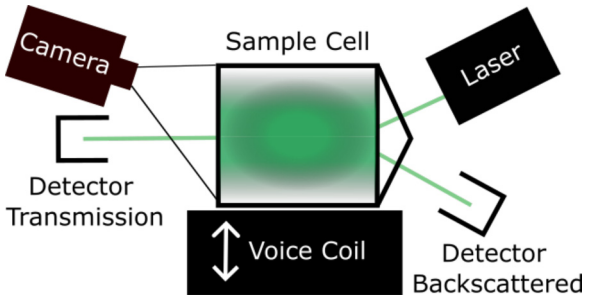

FIG. 1. Schematic of the setup with a sample cell mounted on a voice coil for excitation and a laser source. Light is collected in transmission and backscattering geometry and then fed into avalanche photodiodes (APDs) and a correlator.

geometry. The signal is then passed into a hardware correlator (ALV 7004). The sample, being mounted on a voice coil, can move vertically via the voice coil's sinusoidal oscillation. In addition, a camera (Panasonic hc-v180) is mounted to perform video surveillance to collect information on the packing fraction. We observe the surface of the fluidized bed and cut out a 2D plane representative of the volume occupied by the particles. This assumes that the surface is homogeneous, which is an error-prone assumption in the beginning of shaking. The image analysis is done using Fiji ImageJ [25].

The experimental procedure is as follows. We vacuum dry the sample, weigh it, and fill it into the sample cell. Afterwards, we start the camera recording, and following that the shaking is started with a constant frequency of 100 Hz at a chosen Γ value by tuning the amplitude (85 μm, 21.4 μm, and 19.5 μm), and almost instantly after the shaking is started the DWS collects data. For reproducibility, we start with a strong excitation to always create a loose system. The system is analyzed for 10 s with the measurement time doubling iteratively until 5120 s.

The time steps are chosen for two reasons: First, DWS needs many scattering events for proper statistics. The statistics become insufficient in the highest three decades measured, thereby measuring at least 1000 times as long as the longest timescale we want to observe is necessary [11]. Second, the system changes over time, and the time steps give insight into the dynamics at different volume fractions of the system.

B. Diffusing wave spectroscopy on oscillated grains

Shaken granular matter is commonly characterized by comparing the gravitational acceleration with the vibrational acceleration using the dimensionless acceleration [4,26–28]

$$\Gamma = \frac{A\,\omega^2}{g} \tag{1}$$

with A the oscillation amplitude, ω the angular frequency, g the gravitational acceleration, and Γ the dimensionless acceleration. For $\Gamma < 1$, particles should not be excited enough to be lifted up or slide along each other, but rather show small oscillations. However, it is observed that real systems with shear show densification [4,28,29], whereas for a critical Γ_c above 1 ($\Gamma > 1$), the particles show relative motion and can

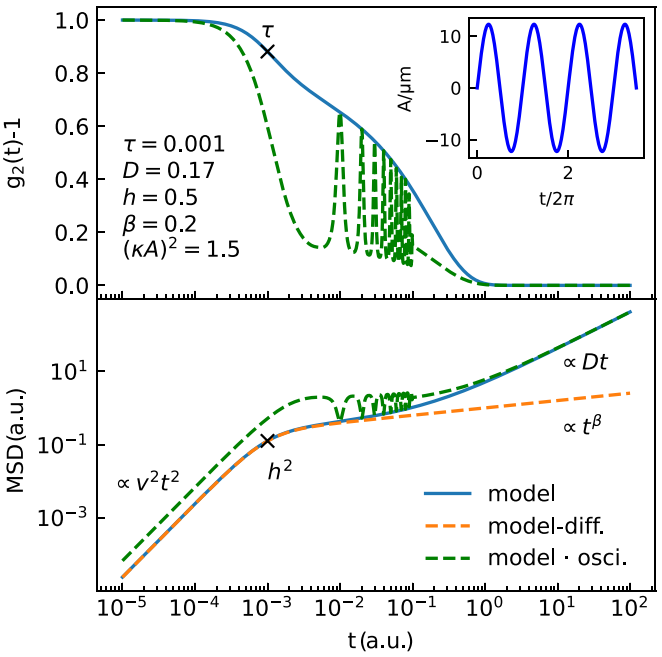

FIG. 2. Depiction of Eq. (10) at arbitrary lag times with a superimposed shaking oscillation. The upper graph shows $g_2(t)$ versus time plot, and the lower one shows the MSD. The dashed green line is a measurement including oscillations, and the blue line is the model function. The orange line depicts a power law attributed to subdiffusive behavior, likely caused by friction or caging. Additionally, the insert shows the sinusoidal oscillation of the voice coil used for excitation.

no longer densify [4]. Shaking a granular packing of frictional spheres will inevitably lead to shear, making it important to note the existence of dilatancy. Shearing a granular packing above a density threshold will make it expand; if below the threshold, the packing will compact [2,30]. For tracking the particle movements, we use DWS as a nonintrusive scattering technique [31,32] illustrated in Fig. 1. The incident laser light undergoes multiple scattering events in the sample before being detected. The fluctuations contain the averaged dynamics of the observed scattering volume and can be correlated to obtain the intensity correlation function $g_2(t)$, defined as

$$g_2(t) = \frac{\langle I(0)I(t)\rangle}{\langle I(0)\rangle\langle I(t)\rangle}. \tag{2}$$

with intensity I. The voice coil used to excite the system is illustrated in Fig. 1, and the sinusoidal excitation is shown in the inset of Fig. 2. The oscillation $O(t)$ is modifying the intensity correlation function $g_2(t)$ as follows:

$$g_{2,\mathrm{mes}}(t) - 1 = O(t)[g_2(t) - 1] \tag{3}$$

with oscillation function

$$O(t) = \frac{1}{T}\int_0^T \exp(-\kappa^2 A^2\{\sin[\omega(t+t')] - \sin(\omega t')\}^2)dt' \tag{4}$$

with the period T, where κ is the variance of the outgoing wave vector projected onto the direction of the oscillation [21]. An estimate for κ can be done assuming that the variance of the accepted scattering vectors is given by the acceptance

angle of the optical fiber setup in the range of 200 μm and an approximate distance of the last scattering event of 100 mm, resulting in $\kappa \approx 0.002k$. The dynamics of the particle are related to the fluctuating electric fields. Assuming the Siegert relation [11],

$$g_2(t) = 1 + \Lambda_{\mathbf{c}} \, |g_1(t)|^2, \tag{5}$$

the intensity correlation function $g_2(t)$ is related to the electric field correlation function $g_1(t)$ (FCF) [11], with the coherence area factor (inverse speckle number) $\Lambda_{\mathbf{c}}$ determining the number of geometrically selected speckles, in our case being one (due to the use of a linear polarizer for the detection) [11]. Assuming the DWS approximation for the electric field correlation function $g_1(t)$ that the light is undergoing a random walk [12] we can relate it to the mean-square displacement (MSD) $\langle \Delta r^2 \rangle$ by

$$g_1(t) = \exp\left[-\frac{1}{3} \left(\frac{kL}{l^*} \right)^2 \langle \Delta r^2 \rangle \right] \tag{6}$$

with $k = 2\pi/\lambda$, the wave vector of the incident light with a magnitude of 1.18×10^9 1/m, L the effective length of the sample, in transmission geometry, the sample length of 5 mm, and 1.43 mm in backscattering geometry [31]. The transmission geometry can be calculated in the framework of the theory. However, backscattering is more complicated and therefore needs to be approximated by an effective length, in relation to the transmission geometry. The randomization length l^* is calculated [see Eqs. (7) to (9)] as 480 μm and can be viewed as the distance until the direction of light propagation is randomized, r is the 3D distance a particle moves, and $\langle\,\rangle$ indicates an ensemble average [11,12]. The randomization length is given by

$$l^* = \frac{l}{1 - \langle \cos(\theta) \rangle} \tag{7}$$

where l is scattering mean-free path and $\langle \cos(\theta) \rangle$ describes the anisotropy of a scattering event. The experimental determination is difficult [33], and we will assume that the surface scattering is, in good approximation, negligible and that, since l^* is small compared to the light paths, backscattering effects are negligible so that transmission and backscattering geometry are treated the same. The distance between scattering events is proportional to the inverse of the number density of the scatterers, ρ_N, multiplied by scattering cross section σ:

$$l(\sigma) = \frac{1}{\rho_N \, \sigma}. \tag{8}$$

This is dependent on the ratio of the wavelength of the incident light to the particle size, according to Mie-Theory [34] and calculated by using the Python program PyMieScatt [35]. In our case, the particles' radii are larger than the wavelength of the light, but not sufficiently large to consider Fraunhofer or geometrical optics. According to Mie theory, backscattering and forward scattering will have different intensities. The volume fraction is given by

$$\Phi = N \, \rho_N = \frac{4\,\pi}{3} \frac{a^3 \, N}{V_{\text{Cell}}} \tag{9}$$

with particle number N and spherical particles with radius a occupying a cell volume V_{Cell}. The particle dynamics can now be extracted by empirically modeling the dynamics with power laws in the MSD representation for the three expected behaviors, ballistic, caging, and diffusion, by

$$\langle \Delta r^2 \rangle = \frac{h^2}{\left(\frac{\tau}{t}\right)^2 + \left(\frac{\tau}{t}\right)^\beta} + 6Dt - 6D\tau(1 - e^{-\frac{t}{\tau}}) \tag{10}$$

with the diffusion coefficient D, ballistic timescale τ, and height h related to the power law describing the caging, taken where the diffusion behavior of the system appears. The first term in Eq. (10) is a ballistic and caging power law, the second term is the diffusion power law, and the third term is a correcting term for the nonadditive contribution of the ballistic and caging power law with the diffusion power law. This ensures that no diffusion contribution appears before the ballistic regime ends. The measured intensity correlation function $g_{2,\text{mess}}$ can be calculated by applying the model Eq. (10) in Eq. (6) and using Eq. (2) to obtain the result shown as the green dashed line in Fig. 2. The blue line describes the particle dynamics by $g_2(t)$ without the oscillations. We use this function to extract the velocity at short timescales, the supposed caging length at intermediate timescales, and diffusing behavior at long timescales. Following that, DWS averages over relative motions of the entire sample volume since the interference pattern is made of components from everywhere in the sample, the MSD values are averaged, and measured velocities are the mean velocities $\overline{v} = v/h$ of fluctuating particles. The velocity fluctuation from the MSD

$$\lim_{t \to 0} \langle \Delta r^2 \rangle = \langle \delta v^2 \rangle t^2 = \overline{v}^2 t^2 \tag{11}$$

is related to the granular temperature [15]

$$T_{\text{Gran}_i} = m\overline{v_i^2} = \tfrac{1}{3}\, m\overline{v}^2 \tag{12}$$

with m the particle mass and v_i the velocity component of one of the three directions in 3D space [2,10,14].

Furthermore, with the velocity, we can estimate the possible deformation and collision time of the particle. For two spherical particles forming and breaking contact, the surface deformation and collision times can be calculated according to Hertz [36–38]. The first important parameter is the elastic modulus (E) of the two spheres colliding, giving the parameter $\Lambda \propto 1/E$ [37]. Using Λ and the radius of the particle a the spring constant of the contact can be calculated as [37]

$$k^2 = \left(\frac{4}{5} \frac{2}{3\Lambda} \right)^2 a. \tag{13}$$

Following this we can use the velocity calculated by DWS ($\overline{v}$), the mass of a particle (m_p), and the following equation to calculate the contact time [37]:

$$t_c = 2.94 \left(\frac{m}{\sqrt{\left(\frac{4}{5}\frac{2}{3\Lambda}\right)^2 R}} \right)^{2/5} \overline{v}^{-1/5} = 2.94 \left(\frac{m}{k} \right)^{2/5} \overline{v}^{-1/5}. \tag{14}$$

Afterward, we can place the indentations caused by the collision in the MSD graphs according to $\delta^2 = (t_c\,\overline{v})^2$.

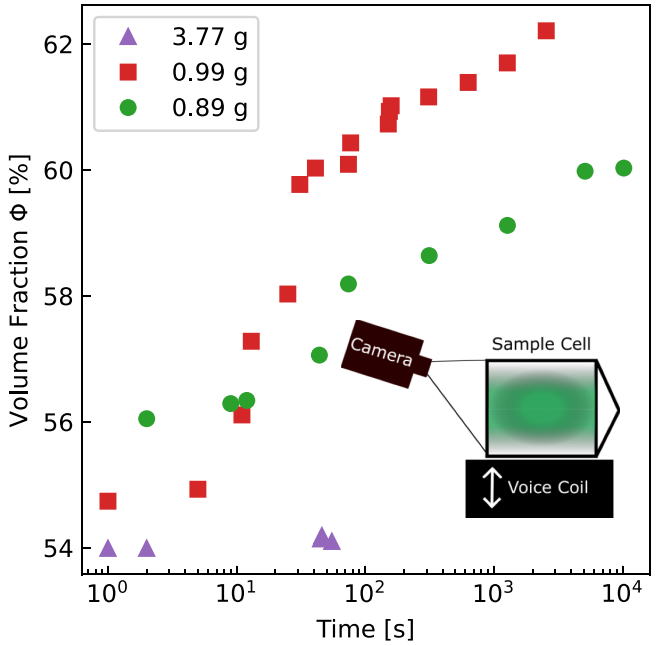

FIG. 3. Evolution of the volume fraction for different Γ values. The volume fraction in percent is plotted versus time to observe any densification. Shaking up is shown in purple triangles and lasts a maximum of 60 s.

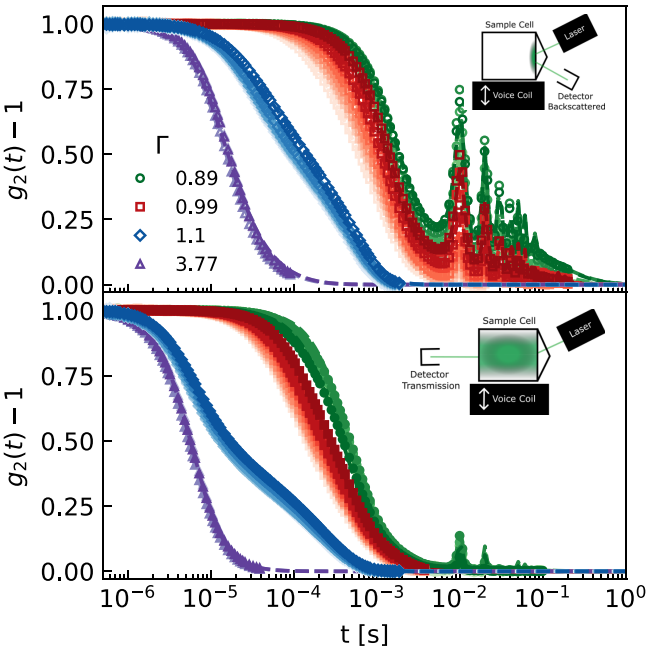

FIG. 4. Γ- and time-dependent Correlation functions $g_2(t)$ in backscattering (top) and transmission (bottom) geometry, with inserts depicting the probed volume. The Γ values of 3.77, 1.1, 0.99, and 0.89 are shown by the purple, blue, red, and green curves, respectively. The color scheme is designed such that darker shades of the color indicate later or denser versions of the same system. Hollow symbols show backscattering values, and full symbols show transmission data.

III. RESULTS

A. Packing fraction

The packing fraction is determined by means of video microscopy during shaking. Determination of the packing fraction using this method can show densification throughout the experiment, which is further supported by changes in the correlation functions seen in Sec. III B. Figure 3 shows the relationship between packing or volume fraction and time. The accuracy can be observed by the grouping of the data and is lower at the beginning of the measurements, as the system still has a more heterogeneous surface in the beginning. As expected, the system densifies over time for both Γ values around 1. The shaking up ($\Gamma = 3.77$) does not further compact the sample. The plateau for $\Gamma = 0.89$ can be explained by the dilatancy onset for monodisperse spheres at $\Phi_D \approx 60\%$ depending on friction and pressure, and this Γ value does not supply enough energy to rearrange the beads and further densify the system [30]. In contrast, the system becomes denser with $\Gamma = 0.99$ as agitation continues. We base this on the same reasoning, as the particles should be able to move relative to each other at Γ_c and become somewhat fluid-like. This can densify the system even above the threshold of $\Phi_D \approx 60\,\%$.

B. Dynamics

Figure 4 shows Γ- and time-dependent correlation functions $g_2(t)$ in backscattering (top) and transmission (bottom) geometry. The purple, blue, red, and green curves show Γ values of 3.77, 1.1, 0.99, and 0.89, respectively. Recorded data are shown as symbols and the fit as lines, showing a good agreement between the fit function and data. The setup depictions in the figures indicate the probed scattering volume. The oscillations look more pronounced in the backscattering correlation functions, and the time is shorter for transmission geometry across all measurements to fully decay. Both factors are not necessarily representative of stronger underlying oscillation amplitudes as well as faster or slower underlying dynamics, respectively.

IV. ANALYSIS

Figure 5 shows Γ- and time-dependent MSDs calculated from data in Fig. 4 shown as symbols and model fits following Eq. (10) shown as dashed lines. The data rely on the determination of the scattering cross section σ, which uses the density determination in Fig. 3. The fitted factor before the oscillation term $\kappa^2 A^2$ is between 0.5 and 1.5 and therefore in the expected order. Since the model can describe the agitation oscillation, we were able to remove the oscillations present in the MSD representation to an almost oscillation-less depiction. The remaining oscillation visible in the MSD curves indicates the level of reliability of the results. The measured MSDs reveal the presence of power-law behavior, initially manifesting as a power-law exponent of 2 at very short timescales, indicative of ballistic motion or elastic deformation. Subsequently, a transition occurs into a plateau-like interval, which may represent caging behavior, gradually softening the cage and exploring a distribution of different ballistic environments. The dots in the lower graph indicate collision times and indentations calculated by the Hertzian model, while the blue

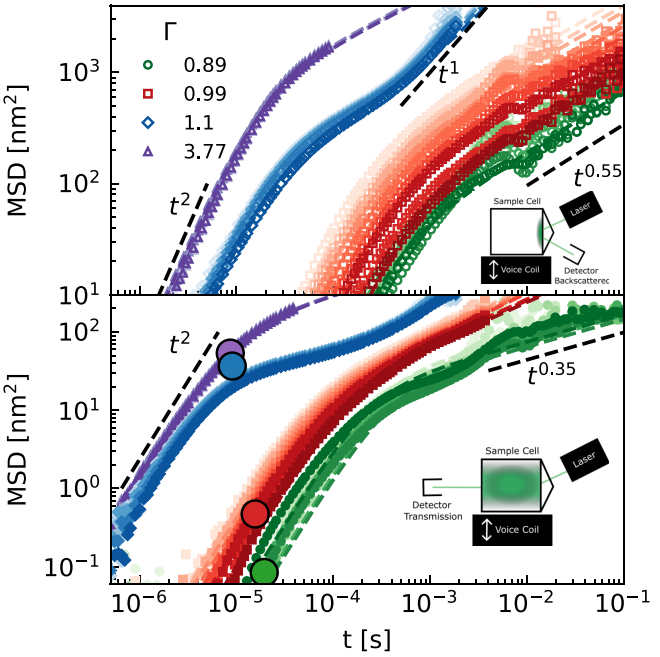

FIG. 5. Γ- and time-dependent MSDs calculated from data in Fig. 4 in backscattering (top) and transmission (bottom) geometry and model fits following Eq. (10). The Γ values of 3.77, 1.1, 0.99, and 0.89 are shown by the purple, blue, red, and green curves, respectively. The color scheme is the same as previously, with empty symbols being backscattering and full ones transmission geometry. The shading indicates the change in volume fraction. The dots in the lower graphs show the lengths and times calculated by assuming Hertzian contacts.

curves ($\Gamma = 1.1$) additionally show a power-law exponent of 1, which is indicative of diffusive motion. For progressively more dense systems, like the red curves, the diffusion is at a later time and has higher displacement values than the technique can resolve. Conversely, the purple curves show no diffusion since the strong agitation has ballistically displaced the particles too far to resolve any particle interactions seen by a full decorrelation before any plateau has formed. To highlight the differences in traveled distances Fig. 6 shows a combined graph of all Γ values at their respective highest achieved volume fraction in backscattering and transmission geometry. It is demonstrated that the backscattering and transmission geometries exhibit a high degree of similarity in shape, with a divergence occurring at the point where the ballistic regime ends. We attribute this to inhomogeneities in the sample. The transmission curves have a lower MSD value than the backscattering curves, suggesting a shorter particle displacement traveled. We expected that the transmitted light experiences a greater exposure to the bulk of the material, thereby providing an average dynamics of the entire sample. Meanwhile, the backscattered light probes the sample closer to the walls. This point is highlighted by the small sample depictions in the figures, where the green color represents the scattered light. The packing differs close to the wall compared to the bulk since the wall prevents proper close packing.

The extracted fit parameters are plotted against volume fraction in Fig. 7, with empty symbols for backscattering

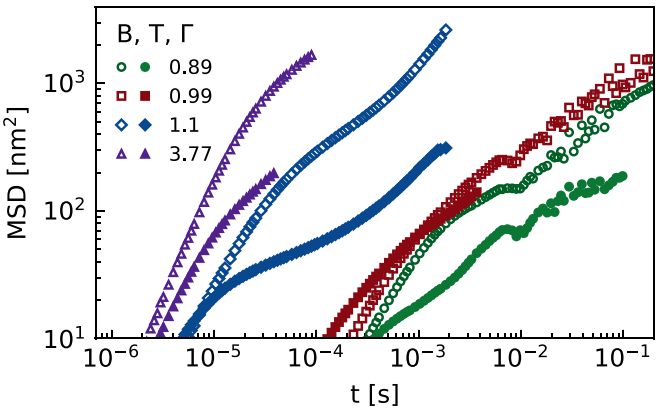

FIG. 6. Γ- and time-dependent MSDs in both geometries joined for all Γ values at their respective initial and highest achieved volume fraction. The backscattering geometry has hollow symbols and transmission full ones. The legend is to be read as a table.

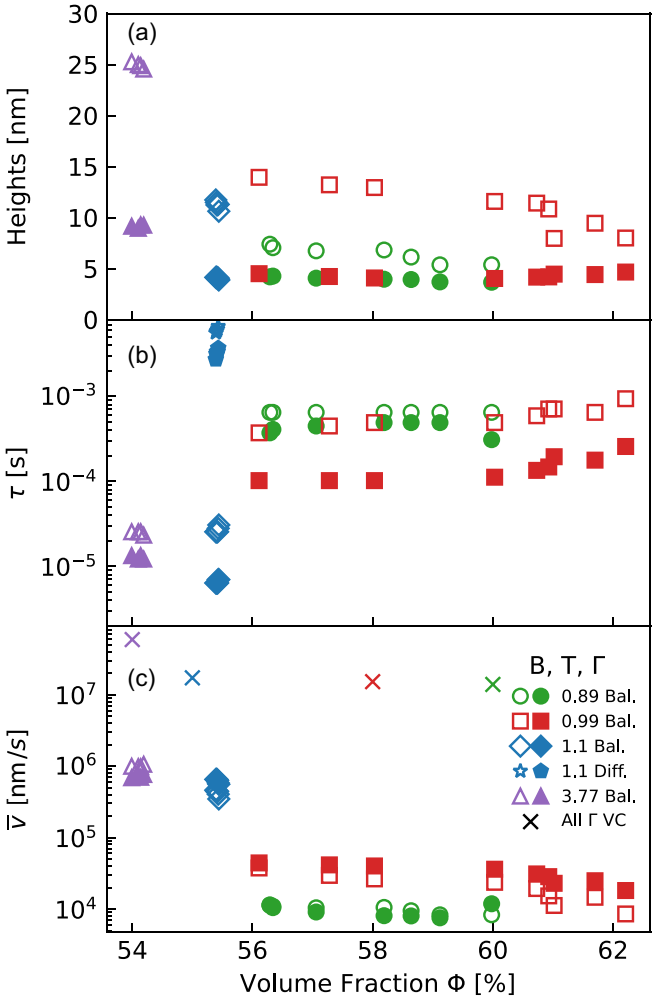

FIG. 7. Extracted correlation times for ballistic motion τ and diffusive motion as well as ballistic particle velocity v and plateau values h by fitting of Eq. (10) to data in Fig. 4. Empty symbols for backscattering geometry and full symbols for transmission geometry. The stars show the diffusion timescale. The legend is to be read as a table.

geometry and full symbols for transmission geometry. The fit parameters h and τ_{Bal} are lower for transmission than for backscattering geometry. The plateau heights decrease with lower excitation energies in the backscattering case, as shown in Fig. 7(a). The backscattering for 1.1 Γ does not follow this trend, and we expected the plateau to be higher. As the system's density increases, the particles enter the caging regime earlier, a phenomenon that can be quantified by observing the decrease in height strongly seen in the backscattering case. The h values for transmission seem to remain constant. This is because the system is more loosely packed close to the wall due to the wall acting like a "surface" breaking the bulk, and the packing fraction can change more drastically there [39]. Ballistic timescales are visible in Fig. 7(b) and show a slight increase as the system densifies for $\Gamma < \Gamma_C$, indicating that the system is becoming slower. Both the backscattering and transmission cases show that the ballistic timescale increases with lower energy input or Γ values. $\Gamma = 1.1$ in transmission does not align with the trend. The diffusive timescales τ_{Diff} are visible only in the blue MSD curves and are shown by the star symbols. The velocities, shown in Fig. 7(c), are calculated according to Eq. (11) and show the expected behavior, as it increases with excitation energy and additionally decreases with density, which is shown by the red and green symbols. The highest Φ value for 0.89 Γ in Figs. 7(b) and 7(c) do not follow the trend exactly, indicating the limits of the data. These deviations reveal the resolution limits indicated by the scattering of the obtained values.

V. DISCUSSION

The system densifies over agitation time, as shown in Fig. 3. This is to be expected as vibrations are a commonly used and highly effective way to densify granular media [40,41]. It can also be seen that the system stops densifying at the dilatancy onset for excitations below $\Gamma = 1$. This phenomenon can be attributed to the inherent difficulty of particle movement relative to each other, thereby hindering the potential for reorientation-driven densification. Higher excitations do not show this property, especially since $\Gamma = 3.77$ visibly fluidizes the sample and has a measured volume fraction below 54%, which is close to the loosest solid granular packing [30,42]. Furthermore, we are aware of the fact that depending on humidity and material used, the system tribo-charges more or less strongly [24,43,44]. In the video recordings, no strong charging effects, e.g., particles sticking to the walls, are visible as the system proceeds to be densified over time. Only the very first measurement showed some effects which could be reasonably attributed to charging, which could have been caused by preparing the sample and filling the sample cell. This leads us to believe that the sample is weakly tribo-charged.

We also observe a clear difference between backscattering and transmission measurements for excitations close to and above $\Gamma = 1$. This leads us to conclude that the system is strongly heterogeneous. At low Γ values this behavior is less prominent. We suspect convection rolls to be one of the causes of this effect, confirmed visually via the video taken of the system [10]. Due to the nature of the scattering geometry, the transmission measurements provide us with a more complete insight into the average behavior of the bulk, as the scattering path passes through the whole sample. This has the benefit of reducing the effect of localized velocity differences in the sample.

From the fits of the MSD curves in Fig. 5, we extract parameters that align with what the MSD curves show by visual inspection. The power-law exponent β, indicative of the slope of the MSD after the ballistic regime, has a constant value of 0.55 for backscattering geometry but differs between excitations for transmission. A β of 0.55, called subdiffusive motion, is not uncommon for colloids in solution [45]. This leads to the assumption that the observed behavior is analogous to a thermal system and thus may indicate caging behavior [45–49]. In general, an exponent of 0.5 is found in strongly collective dynamics for molecular substances and is assumed to be a generic feature of structural relaxation [50,51]. The power law has slight variations between measurements, and this could be caused by the small amount of polydispersity of our system as colloidal DWS measurements with mono- and polydisperse particles show similar characteristics [12,14,52]. Estimation shows that this behavior is influenced by the frictional forces between the particles, and that tuning the friction would change the power-law exponent [30,53,54].

The MSD is cut at the resolution limits given by k; mean distances larger than k cannot be resolved. The calculated MSDs and the limits align well with literature over several decades [13,14]. The resolution limit, however, is given not only in distance but also in time. This leads us to two likely explanations of the cause of the initial ballistic decorrelation. DWS is a statistical average of all dynamics in the scattering volume. As our system has several thousand particles in motion, each one of them needs to move only a fraction of what is given for the one-event decorrelation case.

First, we consider the clapping contacts mentioned in literature on granular media [55,56]. Here contacts would form due to collisions, and these would then deform the particles up 10 nm, when assuming Hertzian contacts, and break apart again [4,36–38,57]. The collision process takes roughly 5×10^{-6}s for our particles at the highest agitation, and slight deviations depend on the excitation energy [37]. It should be noted that the timescale relating to each contact time for each agitation aligns with the ballistic-like increase in the MSD and continues even after the Hertzian contact is expanded. The behavior appears ballistic since the resolved Hertzian part of the MSD is linear following Hook's law, and nonlinear deviations from ballistic behavior should be on even shorter unresolved times. Additionally, the indentations created by making that contact align with the MSD values, making it plausible that the short-timescale behavior analyzed is the contact formation breaking of the Hertzian contact. Lower excitations lead to a bigger deviation from the Hertzian model since the particles are no longer breaking apart, but follow the movement of the voice coil. Interestingly, data of Scalliet *et al.* [58] for very high excitations can be used to extrapolate our data, showing that the actual ballistic behavior happens at slightly larger time and length scales than probable by DWS with green light [58].

Second, it could be either translational or rotational motion of the particles or a combination of both. As the movement on a nanometer scale is very small compared to the size of our particles, one could also attribute the decorrelation to rattling

or vibrations [4]. 1 Å is also equal to 0.01% of a particle's circumference, implying that the amount one particle would need to turn to decorrelate the light path is achievable, even at short timescales.

The surface is assumed to be a strong scattering source, giving us information about the motion of the particle surface (leading to sensitivity for deformation, translation, and rotation). Since the largest refractive index gradient is at the air-particle boundary, the light is scattered weaker on the particle length scale relative to the surface roughness. This can be further illustrated by the observed brightness of each sphere compared to other materials [59,60] and leads to a slight underestimation of l^* resulting in smaller MSDs than assumed.

Measured particle velocities are lower than the velocity of the voice coil, as they should be when considering dissipation; consequently, the excitation itself is not responsible for decorrelating the light. The velocities for high voice coil excitations agree with measurements for granulates falling through a funnel, as both show a mean velocity fluctuation of 0.1–1 mm/s. [13,14]. We measure MSD plateau values between 3×10^1 and 3×10^3 for transmission and backscattering, respectively. The funnel experiment shows a plateau value of roughly 10^3 for particle sizes of 95 μm and 194 μm, covering larger and smaller particle sizes than ours [13]. In the gas-fluidized bed, the plateau is a little below 10^4; this intuitively makes sense as a gas-fluidized bed will be less dense than our system and the particles should have a higher mean-free path [14]. We like to emphasize that the funnel experiment resolves the beginning of diffusion consistently with applied camera-extracted diffusion values underlining the reliability of the extracted length scales [14]. Our particles show no sign of bubbling, therefore the system would be classified as Group A, according to Geldart [61]. Menon's particles, used in a gas-fluidized bed, would be either class A or B [14]. This leads us to believe that the Geldart classification for fluidized beds should be able to be transformed into a granular temperature-dependent version.

When comparing mode-coupling theory (MCT) calculations to our system, the localization lengths normalized to radius should be around 7.46×10^{-2}; our experiment, however, shows a localization length of 1.3×10^{-3} to 4×10^{-4} in backscattering and transmission geometry, respectively [45,62,63]. It is remarkable that the MCT calculations agree with the Lindemann melting criterion or length and still show a difference in MSD of four orders of magnitude from experimental data [64]. We suspect possible causes to be friction, roughnesses, or deviations from a sphere shape on the order of 1%, as the mentioned MCT calculations are frictionless ideal spears. However, the core spectral characteristics of the MSD graph are evident in both theoretical and experimental contexts [62].

VI. CONCLUSION

We demonstrate that DWS can be used to produce reliable and reproducible MSDs from vibro-fluidized beds, in agreement with the literature for other types of fluidization, such as funnel fluidization and gas fluidization [13,14]. All three regimes, ballistic, subdiffusive, and diffusive, shown in previous granular DWS experiments, can be observed in the present voice coil experiment. It is observed that the diffusive behavior changes to the subdiffusive behavior of the system and undergoes a transition in response to agitation (granular temperature). In addition, we verify that the behavior of the system changes as it densifies, as a denser system slows the dynamics. We expect links to jamming and a granular glass transition as the temperature is constant but the dynamics grow slower. Compared to colloidal systems the mean-free paths appear considerably smaller. Finally, we show that the dynamics observed in the backscattered and transmitted geometries are different, demonstrating the sensitivity of DWS to heterogeneities within the system, specifically between wall and bulk dynamics. Consequently, we conclude that DWS can provide a coherent picture of granular fluids across different agitation mechanisms, as it allows the measurement of particle dynamics independent of the agitation method.

ACKNOWLEDGMENTS

This work was supported by the DLR Space Administration with funds provided by the Federal Ministry for Economic Affairs and Climate Action (BMWK) based on a decision of the German Federal Parliament under Grant No. 50WM1945 (SoMaDy2). We are grateful for discussions with Thomas Blochowicz, Matthias Schröter, Karsten Tell, Till Kranz, and Peidong Yu.

DATA AVAILABILITY

The data that support the findings of this article are not publicly available. The data are available from the authors upon reasonable request.

[1] H. M. Jaeger, S. R. Nagel, and R. P. Behringer, Granular solids, liquids, and gases, Rev. Mod. Phys. **68**, 1259 (1996).

[2] B. Andreotti, Y. Forterre, and O. Pouliquen, *Granular Media: Between Fluid and Solid* (Cambridge University Press, Cambridge, 2013).

[3] J. Duran, *Sands, Powders, and Grains: An Introduction to the Physics of Granular Materials* (Springer Science & Business Media, New York, 2012).

[4] A. D. Rosato and C. Windows-Yule, *Segregation in Vibrated Granular Systems* (Academic Press, New York, 2020).

[5] A. J. Liu and S. R. Nagel, Jamming is not just cool any more, Nature (London) **396**, 21 (1998).

[6] L. Berthier and G. Biroli, Glasses and aging, a statistical mechanics perspective on (Springer, Berlin, 2009).

[7] A.-L. Barabási, R. Albert, and P. Schiffer, The physics of sand castles: Maximum angle of stability in wet and dry granular media, Physica A **266**, 366 (1999).

[8] I. Tomasetta, D. Barletta, and M. Poletto, Correlation of powder flow properties to interparticle interactions at ambient and high temperatures, Particuology **12**, 90 (2014).

[9] E. Ehrichs, H. Jaeger, G. S. Karczmar, J. B. Knight, V. Y. Kuperman, and S. R. Nagel, Granular convection observed by magnetic resonance imaging, Science **267**, 1632 (1995).

[10] R. D. Wildman, J. M. Huntley, and D. J. Parker, Granular temperature profiles in three-dimensional vibrofluidized granular beds, Phys. Rev. E **63**, 061311 (2001).

[11] B. J. Berne and R. Pecora, *Dynamic Light Scattering: With Applications to Chemistry, Biology, and Physics* (Courier Corporation, Toronto, 2000).

[12] E. M. Furst and T. M. Squires, *Microrheology* (Oxford University Press, Oxford, 2017).

[13] N. Menon and D. J. Durian, Diffusing-wave spectroscopy of dynamics in a three-dimensional granular flow, Science **275**, 1920 (1997).

[14] N. Menon and D. J. Durian, Particle motions in a gas-fluidized bed of sand, Phys. Rev. Lett. **79**, 3407 (1997).

[15] M. J. Biggs, D. Glass, L. Xie, V. Zivkovic, A. Buts, and M. Curt Kounders, Granular temperature in a gas fluidized bed, Granul. Matter **10**, 63 (2008).

[16] C. Hanotin, P. Marchal, L. J. Michot, C. Baravian, and S. K. de Richter, Dynamics of vibrated granular suspensions probed by mechanical spectroscopy and diffusing wave spectroscopy measurements, Soft Matter **9**, 9352 (2013).

[17] C. Hanotin, S. Kiesgen de Richter, L. Michot, and P. Marchal, Viscoelasticity of vibrated granular suspensions, J. Rheol. **59**, 253 (2015).

[18] K. Kim, J. J. Park, J. K. Moon, H. K. Kim, and H. K. Pak, Solid-liquid transition in a highly dense 3D vibro-fluidized granular system, J. Korean Phys. Soc. **40**, 983 (2002).

[19] K. Kim, J. K. Moon, J. J. Park, H. K. Kim, and H. K. Pak, Jamming transition in a highly dense granular system under vertical vibration, Phys. Rev. E **72**, 011302 (2005).

[20] V. Zivkovic, M. J. Biggs, and D. Glass, Scaling of granular temperature in a vibrated granular bed, Phys. Rev. E **83**, 031308 (2011).

[21] T. Blochowicz, Jamming in granularen medien, Grundpraktikumsanleitung TU Darmstadt, University of Darmstadt (2015).

[22] C. Mayo, M. Kunzner, M. Sperl, and J. P. Gabriel, Observing the glass and jamming transitions of dense granular material in microgravity, arXiv:2504.04161.

[23] S. Garland, G. Gauthier, J. Martin, and J. Morris, Normal stress measurements in sheared non-Brownian suspensions, J. Rheo. **57**, 71 (2013).

[24] A. Schella, S. Herminghaus, and M. Schröter, Influence of humidity on tribo-electric charging and segregation in shaken granular media, Soft Matter **13**, 394 (2017).

[25] J. Schindelin, I. Arganda-Carreras, E. Frise, V. Kaynig, M. Longair, T. Pietzsch, S. Preibisch, C. Rueden, S. Saalfeld, B. Schmid *et al.*, Fiji: An open-source platform for biological-image analysis, Nat. Methods **9**, 676 (2012).

[26] P. Evesque, E. Szmatula, and J.-P. Denis, Surface fluidization of a sand pile, Europhys. Lett. **12**, 623 (1990).

[27] S. Douady, S. Fauve, and C. Laroche, Subharmonic instabilities and defects in a granular layer under vertical vibrations, Europhys. Lett. **8**, 621 (1989).

[28] P. Eshuis, K. Van Der Weele, D. Van Der Meer, R. Bos, and D. Lohse, Phase diagram of vertically shaken granular matter, Phys. Fluids **19**, 123301 (2007).

[29] C. Laroche, S. Douady, and S. Fauve, Convective flow of granular masses under vertical vibrations, J. Physique **50**, 699 (1989).

[30] M. Schröter, A local view on the role of friction and shape, in *EPJ Web of Conferences* (EDP Sciences, 2017), Vol. 140, p. 01008.

[31] W. Brown, *Dynamic Light Scattering* (Clarendon Press, 1993), Chap. 16.

[32] D. Weitz, J. Zhu, D. Durian, H. Gang, and D. Pine, Diffusing-wave spectroscopy: The technique and some applications, Phys. Scr. **1993**, 610 (1993).

[33] S. Utermann, Friction and diffusive light transport in a granular medium, Ph.D. thesis, Georg-August-Universität Göttingen, 2012, http://hdl.handle.net/11858/00-1735-0000-0006-B54C-1.

[34] G. Mie, Beiträge zur Optik trüber Medien, speziell kolloidaler Metallösungen, Ann. Phys. **330**, 377 (1908).

[35] B. J. Sumlin, W. R. Heinson, and R. K. Chakrabarty, Retrieving the aerosol complex refractive index using pymiescatt: A Mie computational package with visualization capabilities, J. Quant. Spectrosc. Radiat. Transfer **205**, 127 (2018).

[36] H. Hertz, Über die Berührung fester elastischer Körper, J. Reine Angew. Math. **92**, 156 (1881).

[37] N. V. Brilliantov, F. Spahn, J.-M. Hertzsch, and T. Pöschel, Model for collisions in granular gases, Phys. Rev. E **53**, 5382 (1996).

[38] K. L. Johnson, One hundred years of Hertz contact, Proc. Inst. Mech. Eng. **196**, 363 (1982).

[39] J.-F. Camenen, Y. Descantes, and P. Richard, Effect of confinement on dense packings of rigid frictionless spheres and polyhedra, Phys. Rev. E **86**, 061317 (2012).

[40] J. B. Knight, C. G. Fandrich, C. N. Lau, H. M. Jaeger, and S. R. Nagel, Density relaxation in a vibrated granular material, Phys. Rev. E **51**, 3957 (1995).

[41] E. R. Nowak, J. B. Knight, E. Ben-Naim, H. M. Jaeger, and S. R. Nagel, Density fluctuations in vibrated granular materials, Phys. Rev. E **57**, 1971 (1998).

[42] G. R. Farrell, K. M. Martini, and N. Menon, Loose packings of frictional spheres, Soft Matter **6**, 2925 (2010).

[43] T. Itakura, H. Masuda, C. Ohtsuka, and S. Matsusaka, The contact potential difference of powder and the tribo-charge, J. Electrost. **38**, 213 (1996).

[44] L.-S. Lu and S.-S. Hsiau, Mixing in vibrated granular beds with the effect of electrostatic force, Powder Technol. **160**, 170 (2005).

[45] G. L. Hunter and E. R. Weeks, The physics of the colloidal glass transition, Rep. Prog. Phys. **75**, 066501 (2012).

[46] W. van Megen and H. Schöpe, The cage effect in systems of hard spheres, J. Phys. Chem. **146**, 104503 (2017).

[47] Z. Xing, A. Caciagli, T. Cao, I. Stoev, M. Zupkauskas, T. O'Neill, T. Wenzel, R. Lamboll, D. Liu, and E. Eiser, Microrheology of DNA hydrogels, Proc. Natl. Acad. Sci. USA **115**, 8137 (2018).

[48] F. Cardinaux, L. Cipelletti, F. Scheffold, and P. Schurtenberger, Microrheology of giant-micelle solutions, Europhys. Lett. **57**, 738 (2002).

[49] M. Gruber, G. Abade, A. Puertas, and M. Fuchs, Active icrorheology in a colloidal glass, Phys. Rev. E **94**, 042602 (2016).

[50] F. Pabst, J. P. Gabriel, T. Boehmer, P. Weigl, A. Helbling, T. Richter, P. Zourchang, T. Walther, and T. Blochowicz, Generic

structural relaxation in supercooled liquids, J. Phys. Chem. Lett. **12**, 3685 (2021).

[51] T. Böhmer, F. Pabst, J. P. Gabriel, R. Zeißler, and T. Blochowicz, On the spectral shape of the structural relaxation in supercooled liquids, J. Chem. Phys. **162** (2025).

[52] J. H. van Zanten, S. Amin, and A. A. Abdala, Brownian motion of colloidal spheres in aqueous PEO solutions, Macromolecules **37**, 3874 (2004).

[53] F. P. Bowden and D. Tabor, *Friction: An Introduction to Tribology* (R. E. Krieger Publishing Company, 1982).

[54] G.-J. Gao, J. Blawzdziewicz, C. S. O'Hern, and M. Shattuck, Experimental demonstration of nonuniform frequency distributions of granular packings, Phys. Rev. E **80**, 061304 (2009).

[55] V. Tournat, V. Zaitsev, V. Gusev, V. Nazarov, P. Béquin, and B. Castagnede, Probing weak forces in granular media through nonlinear dynamic dilatancy: Clapping contacts and polarization anisotropy, Phys. Rev. Lett. **92**, 085502 (2004).

[56] S. van den Wildenberg, M. van Hecke, and X. Jia, Evolution of granular packings by nonlinear acoustic waves, Europhys. Lett. **101**, 14004 (2013).

[57] A. Mathey, M. L. Fur, P. Chasle, A. Amon, and J. Crassous, A device for studying elementary plasticity fluctuations in granular media, arXiv:2403.09396.

[58] C. Scalliet, A. Gnoli, A. Puglisi, and A. Vulpiani, Cages and anomalous diffusion in vibrated dense granular media, Phys. Rev. Lett. **114**, 198001 (2015).

[59] P. V. Rysselberghe, Remarks concerning the Clausius-Mossotti law, J. Phys. Chem. **36**, 1152 (2002).

[60] S. K. Nayar, I. Katsushi, and T. Kanade, *Surface Reflection: Physical and Geometrical Perspectives* (Carnegie Mellon University, 1989).

[61] D. Geldart, Types of gas fluidization, Powder Technol. **7**, 285 (1973).

[62] M. Sperl, Nearly logarithmic decay in the colloidal hard-sphere system, Phys. Rev. E **71**, 060401(R) (2005).

[63] M. Sperl, W. T. Kranz, and A. Zippelius, Single-particle dynamics in dense granular fluids under driving, Europhys. Lett. **98**, 28001 (2012).

[64] F. A. Lindemann, Über die Berechnung molekularer Eigenfrequenzen, Phys. Z **11**, 609 (1910).